3D mixed boundary elements for elastostatic deformation field analysis

Valérie Cayol, F.H. Cornet

3D Mixed Boundary Elements for Elastostatic Deformation Fields Analysis

Int. J. Rock Mech. Min. Sci. & Geomech. Abstr., **34**, 275-287, 1996.

V. Cayol, [1] and F. H. Cornet [2]

A 3D Boundary Elements Method (BEM) combining the Direct and Displacement Discontinuity (DD) methods is developed for the analysis of elastic deformation fields. It can incorporate realistic surface topographies, pressurized reservoirs of any shape, tensile cracks and shear fractures. For accurate representation of geometries, boundaries are discretized with triangular elements. The Direct method, based on the reciprocal theorem and the solution to Kelvin's problem, is the only BEM for which stresses do not become infinite at corners and edges. Therefore, linear planar elements with nodes at apex shared between adjoining elements have been used for accurate and fast modeling of surface topographies and reservoirs. The DD method, based on the analytical solution to the problem of a single DD, is suitable for modeling fractures. With this method, use of constant planar elements is numerically less costly. A modified row-sum elimination method has been developed to permit discretization of surface topographies with linear elements using the Direct method. The Mixed BEM, herein proposed, is tested on a horizontal pressurized fracture of circular shape embedded in an elastic half-space. This example demonstrates the importance of a proper discretization for improving solution time and accuracy. Finally, intersection between elements of different types is discussed.

NOMENCLATURE

$\mathbf{A}$,	Influence coefficient matrix for the DD method.
A_{ikj},	Influence coefficient of the j^{th} DD component on stress σ_{ij}.
B_{ij},	Influence coefficient of the j^{th} DD component on displacement u_i.
$\mathbf{c}$,	Matrix for the singularity when ψ is on the boundary Γ.
$\mathbf{D}$,	DD vector.
$\mathbf{d}$,	Nodal influence coefficient matrix of tractions on tractions.
$\mathbf{F}$, $\mathbf{f}^l$	Known vectors for the Direct method.
$\mathbf{g}$,	Nodal influence coefficient matrix of tractions on displacements.
$\mathbf{H}$,	Influence coefficient matrix for the Direct method.
$\mathbf{h}$, $\hat{\mathbf{h}}$,	Nodal influence coefficient matrix of displacements and of DDs on displacements.
$\mathbf{L}$,	Influence coefficient matrix for the Mixed BEM.

[1]Laboratoire Magmas et Volcans, UMR 6524, 5 rue Kessler, 63038 Clermont-Ferrand cedex, France, E-mail:*cayol@opgc.univ-bpclermont.fr*

[2]Laboratoire de mécanique des roches, Département de sismologie UMR 7580, IPGP, 4 place Jussieu, Boite 89, 75252 Paris Cedex 05, France, E-mail: *cornet@ipgp.jussieu.fr*

n^e, Number of function nodes on element e.
N, Total number of elements.
N_M, Number of elements on massive parts.
N_F, Number of elements and function nodes on fractures.
N_L, Number of function nodes on massive parts.
N_V, Number of function nodes of the virtual complementary boundary
$\mathbf{P}, \mathbf{p}$, Traction vectors.
$\mathbf{R}$, Known vector for the Mixed BEM.
R, Θ, Z, Cylindrical coordinate system.
r, Distance from calculation point ψ to field point t.
$\mathbf{s}$, Nodal influence coefficient matrix of displacements and DDs on tractions.
t, Field point.
$\mathbf{U}, \mathbf{u}$, displacement vectors.
$\mathbf{X}$, Vector of all displacements on massive parts and of all DDs on fractures.
x, y, z, Local Cartesian coordinate system.
x_1, x_2, x_3, Global Cartesian coordinate system.
Γ, Boundary of the body.
Γ_e, Surface of element e.
Γ_F, Boundary of fractures.
Γ_M, Boundary of massive parts.
Γ_V, Virtual complementary boundary.
Γ_δ, Γ'_δ, Boundaries of small hemi-spherical surfaces.
Γ_ϱ, Far field boundary.
Ω, Volume of the body.
ψ, Calculation point (load point for the Direct method).
σ, Stress tensor.

Equations are written in Cartesian coordinates with axes (x_1, x_2, x_3). The i^{th} coordinate of a point t is written $x_i(t)$, vectors and matrices are represented with bold letters, and the i^{th} component of a vector $\mathbf{u}$ is written as $(\mathbf{u})_i = u_i$. $\mathbf{u}^T$ represents the transposed of $\mathbf{u}$. $I_{,i}$ is the partial derivative of function I with respect to x_i. Einstein convention of summation is employed.

INTRODUCTION

Rock engineering problems have been faced in mining, civil or petroleum engineering undertakings. Most of the times, solution to such problems requires, in its first step, an elastic analysis of the stress and/or the displacement field. In many cases, even if the rock mass is homogeneous, mechanical properties of a few major geological discontinuities affecting the site require that these discontinuities be explicitly taken into account [1].

Similar problems are encountered in vulcanology and seismotectonics. Presently, there is a need to apply rock engineering principles to help appraise such environmental hazards. One of the major tools for monitoring volcanic and seismotectonic activity is to measure ground surface deformations. Mechanical models are used to determine the characteristics of the sources of these deformations, and to understand movements of magma [2] or stresses redistribution after earthquakes [3]. In this work, static deformations are considered, as technics used for measuring surface deformations (geodesy, tiltmetry, radar interferometry ...) usually provide discontinuous data. Also, effects of temperature and poroelasticity are neglected.

In order to interpret measured surface deformation fields, several elastic models have been proposed. Mogi [4] developed an analytical formulation for surface displacements created by the inflation of a deep magma body of spherical shape in an elastic half-space. This widely used model is based on the assumption that the size of the sphere is small as compared to the depth of burial. Dieterich and Decker [5] made the first finite element model in vulcanology for calculating ground displacements associated with magma reservoirs of various shapes and dikes of various inclinations in an elastic half-space. They used axisymmetric and plane strain models. 2D boundary elements were used by Pollard and Holzhausen [6] for analyzing surface displacements due to a fluid-filled crack interacting with the free surface. Okada [7] derived analytical expressions for the surface deformation created by inclined shear and tensile faults in an elastic half-space for both point and finite rectangular sources. Displacements are supposed constant on the fault.

These half-space models are widely used for volcanoes where surface topography can be considered flat, like Kilauea in Hawaii, or Kraftla in Iceland. For these volcanoes, effects of irregularities of the ground surface are thought to be too small to be distinguished from errors associated with deformation data. However, for more prominent volcanoes like Mount Etna in Sicilia, Piton de la Fournaise in Réunion Island or Merapi in Indonesia, the general and local aspects of the ground surface critically affect the deformation field [8]. In these cases, realistic topography must be incorporated in the model. Also, for tectonically active regions, use of a half-space model may be justified in strike-slip regime associated with a flat topography, for instance around San Andreas Fault. However, in dip-slip faulted areas, topographic relief is usually significant, and quantitative interpretation of deformations should take it into account. Note also that new surveying techniques like radar interferometry provide global images of ground surface deformations. For prominent topographies, proper interpretation requires a 3D tool.

For this purpose, a fully 3D BEM has been implemented for modeling elastic deformations. With this numerical method,

- real surface topographies can be taken into account,
- the perturbation due to inflation or deflation of reservoirs of any shapes can be modeled,
- tensile cracks as well a shear faults can be incorporated,
- gravitational loads are not dealt with, only the perturbation of the initial state of stress is considered.

For the problems addressed here, the prescribed boundary conditions are tractions. They are null on surface topographies, and equal to the driving pressure on pressurized structures. Shear forces can also be imposed on fractures. For a better approximation of shapes, triangular elements are used. Throughout this paper, surface topographies and pressurized reservoirs are referred to as massive structures. First, principles of the Direct method [9, 10, 11, 12] and the DD method [13, 14, 15, 16] are recalled. Then, motivations for combining the Direct method with linear elements and the DD method with constant elements are discussed and the procedure used to combine these two BEM is explained. This Mixed method is tested and the sensitivity of discretization discussed. Finally, the case of a fracture intersecting a massive structure is presented.

WHY MIXED BOUNDARY ELEMENTS ?

The Direct method

Formulation of the Direct method [9] is derived from Betti's theorem. For an elastic body Ω with boundary Γ, it can be written

$$\int_\Gamma \left(u_j^1(t) p_j^2(t) - u_j^2(t) p_j^1(t) \right) d\Gamma(t) = 0 \ , \tag{1}$$

where u_j and p_j represent j^{th} components of displacement and traction, and superscripts 1 and 2 stand for two different boundary problems. Boundary problem 1 corresponds to the current problem and boundary problem 2 corresponds to Kelvin's problem of a point load in an infinite body. Displacement in direction j at field point t of boundary Γ due to a unit point load acting along x_i at load point ψ inside an infinite body is given by

$$U_{ij}(\psi, t) = \frac{1}{16\pi G(1-\nu)} \frac{1}{r} \left\{ (3-4\nu)\delta_{ij} + r_{,i}\ r_{,j} \right\} \ , \tag{2}$$

where G and ν are elastic constants, δ is the Kronecker's delta function, r is the distance from ψ to t. $r_{,i}$, the partial derivative of r with respect to the field point t, is given by

$$r_{,i} = \frac{x_i(t) - x_i(\psi)}{r} \ .$$

Traction is determined from differentiation of (2) and Hooke's law,

$$P_{ij}(\psi, t) = -\frac{1}{8\pi(1-\nu)} \frac{1}{r^2} \left\{ \left[(1-2\,\nu)\delta_{ij} + 3\, r_{,i}\ r_{,j} \right] \frac{\partial r}{\partial n} - (1-2\,\nu)(r_{,i}\, n_j - r_{,j}\, n_i) \right\} \ , \tag{3}$$

where

$$\frac{\partial r}{\partial n} = (\mathbf{g}rad\, r\,).\mathbf{n} = r_{,i}\ n_i \ ,$$

and $\mathbf{n}$ is the outward unit normal to the surface at t.

For a load point ψ on the surface Γ of the body Ω, a limiting form of Betti's Theorem (1), as ψ goes to the boundary Γ [9, 10], can be written

$$c_{ij}(\psi) u_j(\psi) + \int_\Gamma P_{ij}(\psi, t)\, u_j(t) d\Gamma(t) = \int_\Gamma U_{ij}(\psi, t)\, p_j(t) d\Gamma(t) \ , \ (i = 1, 2, 3) \tag{4}$$

with

$$c_{ij}(\psi) = \lim_{\delta \to 0} \int_{\Gamma_\delta} P_{ij}(\psi, t) d\Gamma(t) \ ,$$

and Γ_δ is a small hemi-spherical surface centered at ψ, which supplements Γ. If the surface is smooth at ψ, $c_{ij} = \frac{1}{2}\delta_{ij}$.

Numerical implementation of the problem [11, 12] is based on two kinds of approximations: First, geometry of the surface is approximated by N triangular planar elements. Second, surface geometry, displacements and tractions are represented using shape functions of their nodal values. For an arbitrary point t on element e, coordinates are expressed in terms of nodes defining the geometry of the element. Displacements and tractions are expressed in terms of their values at function nodes of element e. They can be supposed constant, or with linear or quadratic variations on the element surface, requiring respectively $n^e = 1, 3$ or 6 function nodes on the element. Writing equation (4) in discretized form for the unit point load successively applied to each of the N_L function nodes of the mesh, the following system is obtained [12] , for $l = 1, ..., N_L$,

$$\mathbf{c}^l \mathbf{u}^l + \sum_{e=1}^{N} (\mathbf{h}_{l1} .. \mathbf{h}_{ln^e})^e \mathbf{U}^e = \sum_{e=1}^{N} (\mathbf{g}_{l1} .. \mathbf{g}_{ln^e})^e \mathbf{P}^e \ , \tag{5}$$

where $\mathbf{U}^e = \left\{ \mathbf{u}^1 .. \mathbf{u}^{n^e} \right\}^T$ and $\mathbf{P}^e = \left\{ \mathbf{p}^1 .. \mathbf{p}^{n^e} \right\}^T$ are the displacement and traction vectors on the n^e function nodes of element e, and $(\mathbf{h}_{lk})^e$, $(\mathbf{g}_{lk})^e$ are 3×3 influence coefficient matrices consisting of integrals evaluated at function node k of element e. Despite singularities in $1/r$ and $1/r^2$ in the fundamental solutions (2) and (3), influence coefficients do not become unbounded when l is on element e. For a constant element, the function node is placed at the centroid, and, for a linear or quadratic element, function nodes are generally placed on the edge of the element in order to reduce the number of unknowns in the boundary value problem (Figure 1).

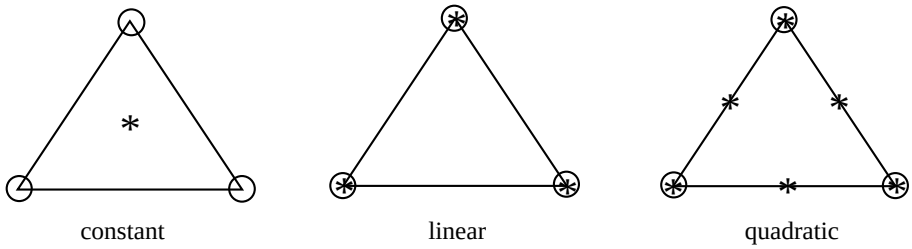

Figure 1: Location of geometrical ($\circ$) and function ($*$) nodes for constant, linear and quadratic Direct method elements

In the actual problem, tractions on elements $\mathbf{P}^e$ are known boundary values. Therefore, the right part of (5) can be calculated. Because the displacement vector at a function node n is unique, the $\mathbf{h}_{lk}$ term of the N_n elements connected to this node can be summed up,

$$\hat{\mathbf{h}}_{ln} = \sum_{r=1}^{N_n} (\mathbf{h}_{lk})^r \ , \tag{6}$$

allowing to replace a sum over elements by a sum over function nodes. Thus, (5) becomes

$$\mathbf{c}^l\mathbf{u}^l + \sum_{n=1}^{N_L}(\hat{\mathbf{h}}_{ln})\mathbf{u}^n = \mathbf{f}^l \ . \tag{7}$$

Finally, unknown boundary displacements are calculated by solving a system of the form

$$\mathbf{H}\ \mathbf{U} = \mathbf{F} \ , \tag{8}$$

where $\mathbf{H}$ is a non-symmetric fully populated influence coefficients matrix, $\mathbf{U}$ represents the $3N_L$ unknown displacements and $\mathbf{F}$ is a known vector of size $3N_L$. This system is solved for $\mathbf{U}$. Solutions at interior points are calculated from Somigliana's identity, which is a form of Betti's theorem corresponding to a unit point load inside the body Ω,

$$u_i(\psi) = -\int_\Gamma P_{ij}(\psi,t)\,u_j(t)d\Gamma(t) + \int_\Gamma U_{ij}(\psi,t)\,p_j(t)d\Gamma(t) \ \ (i=1,2,3) \ . \tag{9}$$

This equation is differentiated and Hooke's law is applied in order to get stresses,

$$\sigma_{ij}(\psi) = -\int_\Gamma S_{ijk}(\psi,t)u_k(t)d\Gamma(t) + \int_\Gamma D_{ijk}(\psi,t)p_k(t)d\Gamma(t) \ . \tag{10}$$

With the identity,

$$\frac{\partial r}{\partial x_i(t)} = -\frac{\partial r}{\partial x_i(\psi)} \ , \tag{11}$$

the third order tensor components S_{ijk} and D_{ijk} are written as,

$$\begin{aligned} S_{ijk}(\psi,t) = \frac{G}{4\pi(1-\nu)}\frac{1}{r^3} \quad & \left\{ 3\frac{\partial r}{\partial n}\left[(1-2\nu)\delta_{ij}r_{,k} + \nu(\delta_{ik}r_{,j} + \delta_{jk}r_{,i}) - 5r_{,i}r_{,j}r_{,k}\right]\right. \\ & +3\nu(n_ir_{,j}r_{,k} + n_jr_{,i}r_{,k}) + (1-2\nu)(3n_kr_{,i}r_{,j} \\ & \left. +n_j\delta_{ik} + n_i\delta_{jk}) - (1-4\nu)n_k\delta_{ij}\right\} \ , \end{aligned} \tag{12}$$

and

$$D_{ijk}(\psi,t) = \frac{1}{8\pi(1-\nu)}\frac{1}{r^2}\{(1-2\nu)(\delta_{ik}r_{,j} + \delta_{jk}r_{,i} - \delta_{ij}r_{,k}) + 3r_{,i}r_{,j}r_{,k}\} \ . \tag{13}$$

Using the approximations previously described for equations (9) and (10), displacements and stresses at interior points are calculated using all boundary values.

The Displacement Discontinuity method

Formulation for the DD method is based on the analytical solution to the problem of a planar element over which material is oppositely displaced [13]. Defining a local coordinate system (x, y, z) such that the z axis is normal to the element plane Γ_e located at $z=0$, the elemental DD corresponds to the following boundary conditions,

$$\left\{ \begin{array}{ll} D_i = u_i^+ - u_i^- & \\ \sigma_{iz}^+ = \sigma_{iz}^- & (i=x,y,z) \ , \end{array} \right. \tag{14}$$

where superscripts + and − indicate values on the positive and negative side of the fracture.

Using harmonic functions, displacements and stresses are expressed as linear functions of the DD components [13]. For constant DD components (D_x, D_y, D_z), the well known expressions [15] for displacements and stresses at point ψ inside the body Ω is obtained:

$$
\begin{aligned}
u_x(\psi) = -\frac{1}{8\pi(1-\nu)} \quad & \{ \quad [z_\psi I_{,xx} - 2(1-\nu) I_{,z}]\, D_x + [z_\psi I_{,xy}]\, D_y \\
& + \quad [z_\psi I_{,xz} + (1-2\nu) I_{,x}]\, D_z \ \} \ , \\
u_y(\psi) = -\frac{1}{8\pi(1-\nu)} \quad & \{ \quad [z_\psi I_{,xy}]\, D_x + [z_\psi I_{,yy} - 2(1-\nu) I_{,z}]\, D_y \\
& + \quad [z_\psi I_{,yz} + (1-2\nu) I_{,y}]\, D_z \ \} \ , \\
u_z(\psi) = -\frac{1}{8\pi(1-\nu)} \quad & \{ \quad [z_\psi I_{,xz} - (1-2\nu) I_{,x}]\, D_x + [z_\psi I_{,yz} - (1-2\nu) I_{,y}] D_y \\
& + \quad [z_\psi I_{,zz} - 2(1-\nu) I_{,z}]\, D_z \ \} \ ,
\end{aligned}
\tag{15}
$$

$$
\begin{aligned}
\sigma_{xx}(\psi) = \frac{G}{4\pi(1-\nu)} \quad & \{ \quad [2I_{,xz} - z_\psi I_{,xxx}]\, D_x + [2\nu I_{,yz} - z_\psi I_{,xxy}] D_y \\
& + \quad [I_{,zz} + (1-2\nu) I_{,yy} - z_\psi I_{,xxz}] D_z \} \ , \\
\sigma_{yy}(\psi) = \frac{G}{4\pi(1-\nu)} \quad & \{ \quad [2\nu I_{,xz} - z_\psi I_{,xyy}]\, D_x + [2I_{,yz} - z_\psi I_{,yyy}] D_y \\
& + \quad [I_{,zz} + (1-2\nu) I_{,xx} - z_\psi I_{,yyz}] D_z \} \ , \\
\sigma_{zz}(\psi) = \frac{G}{4\pi(1-\nu)} \quad & \{ \quad -[z_\psi I_{,xzz}] D_x - [z_\psi I_{,yzz}] D_y + [I_{,zz} - z_\psi I_{,zzz}] D_z \} \ , \\
\sigma_{xy}(\psi) = \frac{G}{4\pi(1-\nu)} \quad & \{ \quad [(1-\nu) I_{,yz} - z_\psi I_{,xxy}]\, D_x + [(1-\nu) I_{,xz} - z_\psi I_{,xyy}] D_y \\
& - \quad [(1-2\nu) I_{,xy} + z_\psi I_{,xyz}] D_z \} \ , \\
\sigma_{yz}(\psi) = \frac{G}{4\pi(1-\nu)} \quad & \{ \quad -[\nu I_{,xy} + z_\psi I_{,xyz}]\, D_x + [I_{,zz} + \nu I_{,xx} - z_\psi I_{,yyz}] D_y \\
& - \quad [z_\psi I_{,yzz}] D_z \} \ , \\
\sigma_{zx}(\psi) = \frac{G}{4\pi(1-\nu)} \quad & \{ \quad [I_{,zz} + \nu I_{,yy} - z_\psi I_{,xxz}]\, D_x - [\nu I_{,xy} + z_\psi I_{,xyz}] D_y \\
& - \quad [z_\psi I_{,xzz}] D_z \} \ ,
\end{aligned}
\tag{16}
$$

where

$$
I = I(\psi) = \int_{\Gamma_e} \frac{1}{r} d\Gamma(t) \ . \tag{17}
$$

r is the distance from point t of Γ_e to ψ. The influence coefficients on stresses contain integrals with singularities of orders $1/r^2$ and $1/r^3$, making stresses at the edge of an element unbounded.

Numerical implementation of the method, [14, 15], is based on the superposition principle that result from linear elasticity. Solution on a fracture of any shape is found by dividing it into N planar triangular elements over which elemental DDs are distributed.

Expressing influences of individual DDs in the global coordinate system (x_1, x_2, x_3) and superposing them, displacements and stresses at $\psi \in \Omega$ are written as a linear combination of all DDs,

$$u_i(\psi) = \sum_{e=1}^{N} B_{ij}^{\psi e} D_j^e \ , \tag{18}$$

$$\sigma_{ik}(\psi) = \sum_{e=1}^{N} A_{ikj}^{\psi e} D_j^e \ , \tag{19}$$

where $B_{ij}^{\psi e}$ and $A_{ikj}^{\psi e}$ represent the influence coefficients at ψ of D_j^e, the j^{th} component of the DD on element e. For traction boundary problems, a system of equations is formed from (19) by expressing the boundary traction at the centroid of every fracture element l. The following system is obtained, for $l = 1, ..., N$,

$$p_i^l = \left(\sum_{e=1}^{N} A_{ikj}^{le} D_j^e \right) n_k^l \ , \tag{20}$$

where n_k^l is k^{th} component of the normal at the centroid of element l. Amplitudes of the $3N$ DDs are adjusted so that they match the prescribed boundary tractions by solving a system of the form

$$\mathbf{P} = \mathbf{A}\ \mathbf{D} \ . \tag{21}$$

$\mathbf{P}$ represents $3N$ prescribed tractions, $\mathbf{A}$ the influence coefficient matrix and $\mathbf{D}$ $3N$ DD components. Finally, boundary displacements as well as displacements and stresses at interior points can be calculated using the DDs amplitudes in equations (18) and (19).

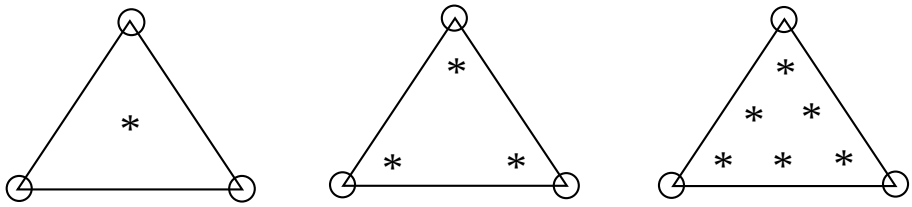

Figure 2: Location of geometrical ($\circ$) and function ($*$) nodes for constant, linear and quadratic DD elements

Expressions have been derived for constant elements. However, if elements with higher-order functional variations were used [16], singularity of stresses on edges of elements would force to place function nodes inside elements (see Figure 2).

Reasons for combining the Direct and the DD methods

When choosing a BEM for modeling deformations, attention should be paid to the following aspects: First, numerical cost of solutions should be minimized. In 3D, large systems of equations are often met which require disk swapping for their resolution. As transmission of data to and from the hard disk is at least 1000 times slower than from the RAM, this process considerably slows down resolution, and solution of the linear

	constant elements	linear elements	quadratic elements
Direct method	N_M	$\frac{3N_M}{6} = \frac{N_M}{2}$	$\frac{3N_M}{6} + \frac{3N_M}{2} = 2N_M$
DD method	N_M	$3N_M$	$6N_M$

Table 1: Number of function nodes required with the Direct and the DD methods for constant, linear and quadratic elements. Geometrical nodes are shared between an average of 6 elements. N_M is the number of elements used for massive boundaries.

system becomes the most time consuming operation. As the size of the linear system is 3 $\times$ (number of function nodes), this number should be minimized. Second, accurate calculation of solutions should be made possible almost anywhere in the elastic medium.

The Direct method as compared to the DD method never involves unbounded coefficients. This has several advantages with regard to massive boundaries:

1. The Direct method is more exact than the DD method when dealing with structures with sharp edges or corners as can be the case with real topographies. Indeed, with the Direct method, boundary integral equations can be written in terms of actual boundary values at function nodes located anywhere on boundaries. This cannot be done with the DD method, where influence coefficients on stresses become infinite at edges of elements.

2. The Direct method with linear or quadratic elements allows calculation of stresses everywhere near and on the boundary. Indeed, with linear or quadratic elements, displacements and stresses are defined everywhere on the elements.

3. For a given discretization of massive boundaries, use of linear elements with the Direct method minimizes solution time. Suppose massive boundaries are discretized with N_M elements. Table 1 shows that, when apex of triangular elements are shared between an average of 6 elements, the Direct method with linear elements requires the least function nodes. Table 1 also shows that, with the DD method, constant elements are the least expensive numerically. Now The Direct method using linear elements requires calculation of $9N_M^2/2$ influence coefficients, whereas the DD method with constant elements requires calculation of $9N_M^2$ influence coefficients. Therefore, for massive boundaries the Direct method is half as costly as the DD method.

However, when modeling fractures, the DD method is more appropriate than the Direct method:

1. For fractures, the DD method with constant elements is numerically as costly as the Direct method with linear elements. If the Direct method is used, boundary elements are required on both sides of fractures. Suppose, fractures are discretized with $2N_F$ elements. If function nodes are shared between an average of 6 elements,

assembly of the system (5) requires calculation of a total of $2 \times 18(N_F/2)^2 = 9N_F^2$ influence coefficients. On the contrary, with the DD method, a fracture is treated as a single surface. For the same level of discretization as with the Direct method, only N_F elements are required on fractures. Thus, only $9N_F^2$ coefficients have to be calculated.

2. It is numerically stable whereas the Direct method will break down when function nodes of two element coincide. In fact, this will lead to equal influence coefficients and will result in an ill-conditioned system.

From the discussion above, it appears that the Direct and DD methods are complementary: The Direct method with linear elements is particularly appropriate when modeling ground surfaces or pressurized reservoirs, whereas the DD method with constant elements is more suitable for fractures. For these reasons, both methods have been combined.

COMBINATION OF THE DIRECT METHOD AND THE DISPLACEMENT DISCONTINUITY METHOD

Description of the method

To combine the DD and Direct methods, the procedure outlined by Diering [17] is generalized. Diering developed a Mixed BEM using constant rectangular elements for analyzing mining excavation in fractured media. Combination of the two methods is derived from the Direct method. Betti's theorem is written for a boundary containing massive parts Γ_M and closed fractures such that the sides $(+)$ and $(-)$ of a fracture are at the same location corresponding to Γ_F. Two cases must be distinguished depending on the boundary where the unit point load ψ is applied:
If $\psi \in \Gamma_M$, (4) gives:

$$\begin{aligned} c_{ij}(\psi)u_j(\psi) \;=\; & -\int_{\Gamma_M} P_{ij}(\psi,t)u_j(t)d\Gamma(t) + \int_{\Gamma_M} U_{ij}(\psi,t)p_j(t)d\Gamma(t) \\ & -\int_{\Gamma_F} \Big(P_{ij}^+(\psi,t)u_j^+(t) + P_{ij}^-(\psi,t)u_j^-(t) \Big)\, d\Gamma(t) \\ & +\int_{\Gamma_F} \Big(U_{ij}^+(\psi,t)p_j^+(t) + U_{ij}^-(\psi,t)p_j^-(t) \Big)\, d\Gamma(t)\ . \end{aligned} \tag{22}$$

If $\psi \in \Gamma_F$, the integral equation is derived by writing Betti's theorem (1) with ψ excluded from the fracture by two half spheres (Figure 3) Γ_δ and Γ'_δ. Then, taking the limit of this expression as $\delta \to 0$, the following equation is obtained for ψ on a planar surface:

$$\begin{aligned} \frac{1}{2}u_i^+(\psi) + \frac{1}{2}u_i^-(\psi) \;=\; & -\int_{\Gamma_M} P_{ij}(\psi,t)u_j(t)d\Gamma(t) + \int_{\Gamma_M} U_{ij}(\psi,t)p_j(t)d\Gamma(t) \\ & -\int_{\Gamma_F} \Big(P_{ij}^+(\psi,t)u_j^+(t) + P_{ij}^-(\psi,t)u_j^-(t) \Big)\, d\Gamma(t) \\ & +\int_{\Gamma_F} \Big(U_{ij}^+(\psi,t)p_j^+(t) + U_{ij}^-(\psi,t)p_j^-(t) \Big)\, d\Gamma(t)\ . \end{aligned} \tag{23}$$

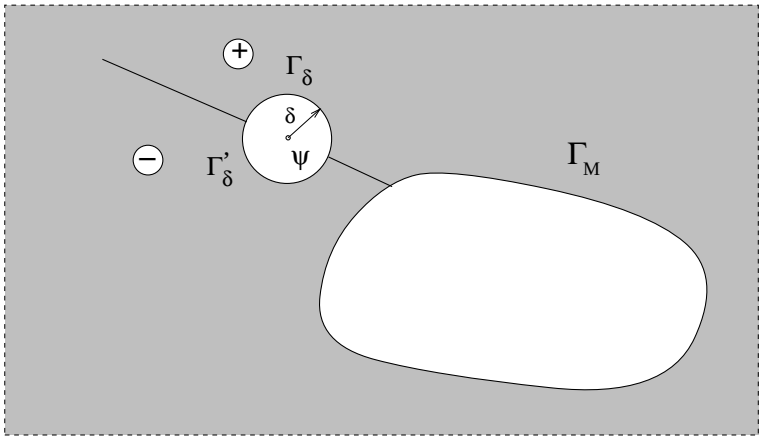

Figure 3: Exclusion of point ψ by 2 half spheres

As seen previously, a DD is such that, across fractures, displacements are discontinuous and stresses are continuous. Since outward normals for the sides $(+)$ and $(-)$ are equal in magnitudes but opposite in signs, (14) yields

$$p_j^+(t) = -p_j^-(t) \ . \tag{24}$$

Also, the sides $(+)$ and $(-)$ are at identical location. From (2) and (3), this implies

$$U_{ij}^+(\psi,t) = U_{ij}^-(\psi,t) \quad \text{and} \quad P_{ij}^+(\psi,t) = -P_{ij}^-(\psi,t) \ . \tag{25}$$

Substituting (24), (25) in (22), (23), and using (14) gives, for $\psi \in \Gamma_M$,

$$\begin{aligned} c_{ij}(\psi)u_j(\psi) &= -\int_{\Gamma_M} P_{ij}(\psi,t)u_j(t)d\Gamma(t) + \int_{\Gamma_M} U_{ij}(\psi,t)p_j(t)d\Gamma(t) \\ &\quad -\int_{\Gamma_F} P_{ij}^+(\psi,t)D_j(t)d\Gamma(t) \ , \end{aligned} \tag{26}$$

and, for $\psi \in \Gamma_F$,

$$\begin{aligned} u_i^+(\psi) &= -\int_{\Gamma_M} P_{ij}(\psi,t)u_j(t)d\Gamma(t) + \int_{\Gamma_M} U_{ij}(\psi,t)p_j(t)d\Gamma(t) \\ &\quad -\int_{\Gamma_F} \left(P_{ij}^+(\psi,t) - \delta_{ij}\Delta(t-\psi)\right) D_j(t)d\Gamma(t) \ . \end{aligned} \tag{27}$$

where Δ is the Dirac delta function.

Equation (27) does not involve boundary tractions on fractures. Therefore, it cannot be used to solve boundary traction problems, and a new equation is required for the expression of tractions on fractures. Stress components at $\psi \in \Gamma_F$ are derived by differentiating (27) and applying Hooke's law. Multiplying the stress tensor by the normal at ψ leads to the following expression for tractions on fractures:

$$\begin{aligned} p_i^+(\psi) &= -n_j(\psi)\left[\int_{\Gamma_M} S_{ijk}(\psi,t)u_k(t)d\Gamma(t) - \int_{\Gamma_M} D_{ijk}(\psi,t)p_k(t)d\Gamma(t)\right] \\ &\quad -n_j(\psi)\int_{\Gamma_F} S_{ijk}^+(\psi,t)D_k(t)d\Gamma(t) \end{aligned} \tag{28}$$

It can be shown [17] that, for constant DDs, the influence coefficients of the DDs obtained in (26) and (28) are the same as those found in (15) and (16) using harmonic functions.

Suppose massive parts are discretized with N_M linear elements having N_L function nodes, and fractures are discretized with N_F constant elements having N_F function nodes. Using the approximations defined previously with the Direct method, (26) and (28) lead to the following system of equations, for $l = 1, ..., N_L$,

$$\mathbf{c}^l\mathbf{u}^l + \sum_{e=1}^{N_L} \hat{\mathbf{h}}_{le}\mathbf{u}^e + \sum_{m=1}^{N_F} \mathbf{h}_{lm}\mathbf{D}^m = \sum_{e=1}^{N_M} (\mathbf{g}_{l1}..\mathbf{g}_{ln^e})^e\mathbf{P}^e \ , \tag{29}$$

and, for $l = N_L + 1, ..., N_L + N_F$,

$$\left[\sum_{e=1}^{N_L} \hat{\mathbf{s}}_{le}\mathbf{u}^e + \sum_{m=1}^{N_F} \mathbf{s}_{lm}\mathbf{D}^m\right] \mathbf{n}^l = \left[\sum_{e=1}^{N_M} (\mathbf{d}_{l1}..\mathbf{d}_{ln^e})^e\mathbf{P}^e\right] \mathbf{n}^l - \mathbf{p}^l \ , \tag{30}$$

After calculating the right hand side of these equations, the system constituted by (29) and (30) is expressed as

$$\mathbf{L}\ \mathbf{X} = \mathbf{R} \ , \tag{31}$$

where, $\mathbf{L}$ is the influence coefficients matrix, $\mathbf{X} = \left\{\mathbf{u}^1..\mathbf{u}^{N_L}\mathbf{D}^1..\mathbf{D}^{N_F}\right\}^T$ represents $3(N_L + N_F)$ unknowns of the boundary value problem, and $\mathbf{R}$ is a $3(N_L + N_F)$ known vector.

Once this system is solved, displacements inside the domain can be calculated using Somigliana's identity (9) written for the boundary with both massive parts and fractures. Considering equalities (24), (25), and the usual approximations, displacements at $\psi \in \Omega$ are

$$\mathbf{u}^\psi = -\sum_{e=1}^{N_L} \hat{\mathbf{h}}_{\psi e}\mathbf{u}^e - \sum_{m=1}^{N_F} \mathbf{h}_{\psi m}\mathbf{D}^m + \sum_{e=1}^{N_M} (\mathbf{g}_{\psi 1}..\mathbf{g}_{\psi n^e})^e\mathbf{P}^e \ . \tag{32}$$

Differentiating this equation and using Hooke's law give stresses,

$$\sigma^\psi = -\sum_{e=1}^{N_L} \hat{\mathbf{s}}_{\psi e}\mathbf{u}^e - \sum_{m=1}^{N_F} \mathbf{s}_{\psi m}\mathbf{D}^m + \sum_{e=1}^{N_M} (\mathbf{d}_{\psi 1}..\mathbf{d}_{\psi n^e})^e\mathbf{P}^e \ . \tag{33}$$

Numerical implementation

The Mixed BEM has been implemented from a preexisting program COMPUTE^{3D} [18, 19, 20] developed by Curran, Corkum and Shah. COMPUTE^{3D} uses the Direct method with triangular planar elements on which solutions may be constant, or have linear or quadratic variations. It was designed for mining, therefore only null boundary values could initially be imposed. Different integrations schemes are combined to calculate influence coefficients of the Direct method. Regular integrals are evaluated with a Gauss-Hammer numerical integration of different orders [22], quasi-singular integrals (corresponding to the case where the function node is located near the elements of integration) are evaluated analytically [23, 24], and singular integrals (the function node is located on the element of integration) are evaluated with a combination of regularizing transformation and row-sum elimination method [12]. Solution of the system of equations

is performed using a General Minimum Residual method [25] as it appears [19] to be the most reliable and numerically efficient way of solving boundary element problems.

Combination of the DD and Direct methods, for the analysis of structures containing fractures, pressurized reservoirs and a ground surface, requires some modifications of COMPUTE^{3D}:

1. New singular influence coefficients $\mathbf{s}_{ll}$ (30), corresponding to the influence of a fracture element on itself, need to be calculated. It is performed analytically from the calculation of I and its derivatives involved in (16) for $z = 0$ (see Appendix).

2. For linear elements of Γ_M, singular influence coefficients of 3×3 matrices $\mathbf{c}^l + \hat{\mathbf{h}}_{ll}$ (29), have to be evaluated with a row-sum elimination method [21] modified in order to account for fractures and the ground surface. The row-sum elimination method allows evaluation of singular influence coefficients in $\mathbf{c}^l + \hat{\mathbf{h}}_{ll}$ without performing integration of singular terms. This is particularly useful at corners, where evaluation of $\mathbf{c}^l$ can be critical in 3D. Note that, if constant elements were used instead of linear elements on massive parts, $\mathbf{c}^l + \hat{\mathbf{h}}_{ll}$ could be calculated analytically. The row-sum elimination method is ordinarily derived from the limiting form of Betti's theorem given in equation (4). Considering the fact that influence coefficients in $\mathbf{c}^l + \hat{\mathbf{h}}_{ll}$ only depend on the geometry of the problem, these coefficients are the same if a rigid body movement with null tractions is imposed to the boundaries instead of the actual boundary values. Now, for a boundary containing a ground surface (i.e. a non-closed surface), conditions of equilibrium are violated. Therefore, Betti's theorem is no longer valid. This difficulty is overcome by implementing the row-sum elimination for the ground surface supplemented by a virtual surface Γ_V (Figure 4). Equilibrium is now respected. Suppose a rigid body displacement $u_j(t) = 1$, with

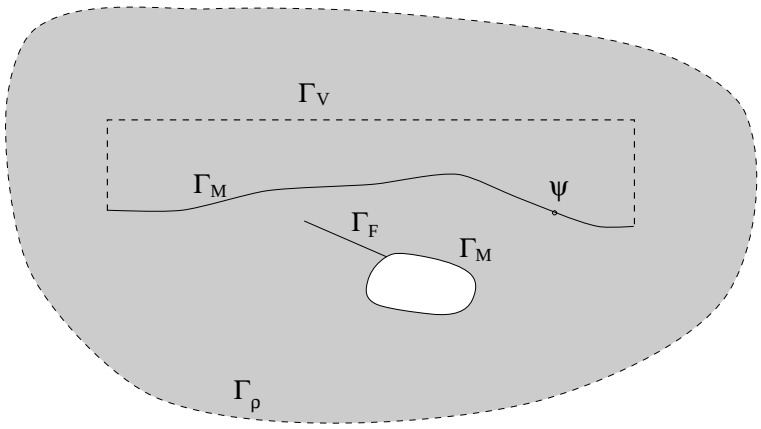

Figure 4: Schematic 2D representation of the boundaries, with a far boundary Γ_ϱ and the ground surface completed by a virtual surface Γ_V.

null tractions $p_j(t) = 0$, is imposed to the body. The modified row-sum elimination method is derived from the limiting form of Betti's theorem (26) written for ψ on massive parts Γ_M of the boundary,

$$c_{ij}(\psi) + \int_{\Gamma_M} P_{ij}(\psi, t) d\Gamma(t) \quad + \quad \int_{\Gamma_V} P_{ij}(\psi, t) d\Gamma(t)$$

$$+ \lim_{\varrho\to\infty} \int_{\Gamma_\varrho} P_{ij}(\psi,t)d\Gamma(t) = 0 \ . \tag{34}$$

The fracture boundary Γ_F does not appear in this equation as amplitudes of DDs, $D_j = u_j^+ - u_j^-$, are null for a rigid body movement. Moreover, since tractions P_{ij} over Γ_ϱ are due to a unit point load, equilibrium of the domain implies

$$\lim_{\varrho\to\infty} \int_{\Gamma_\varrho} P_{ij}(\psi,t)d\Gamma(t) = -\delta_{ij} \ . \tag{35}$$

Thus, when the virtual surface is discretized with N_V function nodes, using the approximations previously defined, (34) and (35) give:

$$\mathbf{c}^l + \hat{\mathbf{h}}_{ll} = \mathbf{I} - \sum_{m=1,m\neq l}^{N_L} \hat{\mathbf{h}}_{lm} - \sum_{q=1}^{N_V} \hat{\mathbf{h}}_{lq} \ . \tag{36}$$

In order to calculate these singular terms at a reduced numerical cost, the virtual surface is composed of large elements. To improve accuracy, integrals on Γ_V are calculated analytically.

Note also that the supplementary contour Γ_V only appears in the row-sum. It is not taken into account when calculating $\mathbf{R}$ in (31) and no unknown of $\mathbf{X}$ is associated to it.

3. The Mixed BEM is modified to permit prescribing fluid pressures. These can be constant, or linearly varying to account for the variation of pressure with depth. This variation may become considerable for a high magma reservoir or a high vertical dyke.

4. In order to handle intersections of massive boundaries with fractures, constant elements are used for parts of massive boundaries adjoining fractures. Actually, if conforming linear elements were used everywhere on massive boundaries, the Mixed BEM would break down as, with the DD method, stresses are singular on elements edges. Therefore, the influence coefficients of nodes shared between a massive structures and a fracture, on stresses of the adjoining DD elements, would be infinite.

VALIDATION OF THE MIXED BEM

Procedure for the validation with a known analytical solution

Validation is performed on a problem with a known analytical solution [26] which is the problem of a pressurized circular horizontal fracture embedded in an elastic half-space (i.e. a flat topography). Characteristics of the model are detailed in Figure 5. Elastic properties are taken as 50 000 *Mpa* for Young's Modulus and 0.21 for Poisson's ratio. These correspond to average values given by Touloukian et al. [27] for basalt. Displacements calculated analytically are compared to numerical results found using the DD method for the fracture and the Direct method for the ground surface. Accuracy of

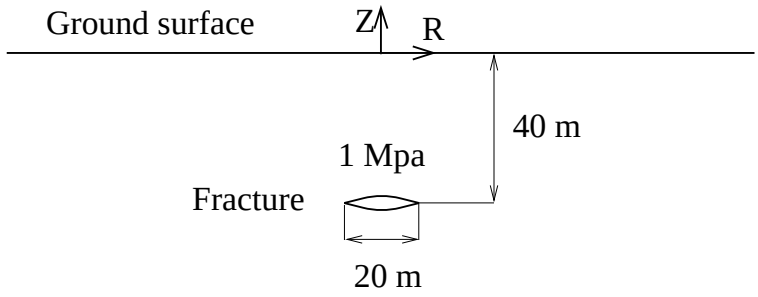

Figure 5: Characteristics of the model used to validate the Mixed BEM

numerical results is estimated by the mean relative error on vertical displacement for the N_{20} function nodes of the ground surface located within 20 m from origin,

$$Err\ u_Z(\%) = \frac{1}{N_{20}} \sum_{R<20} \left| \frac{u_Z^{analytical} - u_Z^{numerical}}{u_Z^{analytical}} \right| . \tag{37}$$

First, combination of the DD and Direct methods is validated for constant elements on which singular influence coefficients $\mathbf{c}^l + \hat{\mathbf{h}}_{ll}$ are calculated analytically. Then, accuracy of the modified row-sum elimination method is verified for massive parts Γ_M discretized with constant elements. This is done by comparing results obtained when singular influence coefficients $\mathbf{c}^l + \hat{\mathbf{h}}_{ll}$ are evaluated both analytically and by the modified row-sum elimination method. Finally, the modified row-sum elimination method is verified for Γ_M discretized with linear elements, by comparing results with those obtained for Γ_M discretized with constant elements.

Validation of the combination of the Direct and DD methods

Results are compared for three different ground surfaces. Two of them are 200 m $\times$ 200 m square surfaces regularly divided respectively in 800 and 1800 triangular elements (Figure 6a and 6b) of equal sizes (respectively 50 m^2 and 22.2 m^2). The third one is a circular surface (Figure 6c) of radius 100 m composed of 820 elements of size gradually increasing from 2 m^2 near the origin to 120 m^2 towards the surface rim. The circular fracture has been modeled respectively with 226 and 638 elements with average sizes respectively of 2.8 m^2 and 1 m^2. For the ground surfaces, it has been verified (by comparing with results from larger surfaces with the same discretizations) that the outer boundary is far enough not to influence results by more than 0.5 % for $R < 50$.

Figure 7 shows that, for the 638 elements fracture and the circular ground surface, numerically calculated displacements slightly overestimate the closed-form solution. In fact, such an overestimation is found for every discretization of the fracture and of the ground surface. Table 2 shows that, for a given discretization of the fracture, the mean relative error (i.e. overestimation) increases when discretization of the square surface is increased. This result is opposite to what is expected. However, when discretization of the fracture is increased, errors diminish. Indeed, when the ground surface is discretized with finer elements, it becomes more "compliant". Thus, it is more sensitive to the perturbation imposed on the fracture. Now, if tractions and displacements are overestimated on the fracture, a more discretized ground surface will reflect these overestimations more

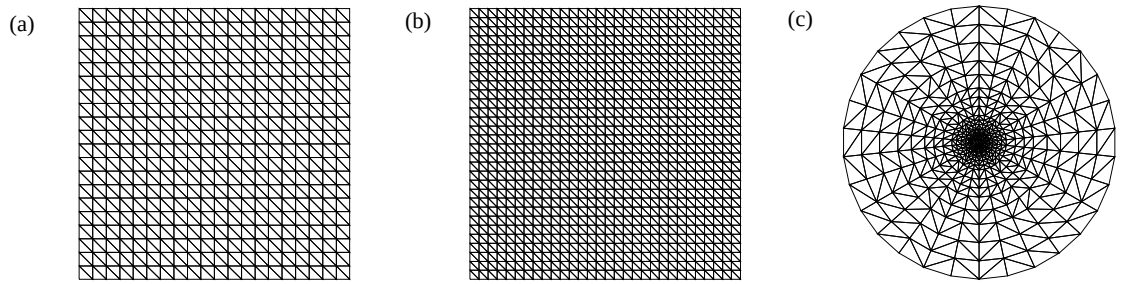

Figure 6: Discretizations for the ground surface. (a) Regular mesh, 800 elements. (b) Regular mesh, 1800 elements. (c) Graded mesh, 820 elements.

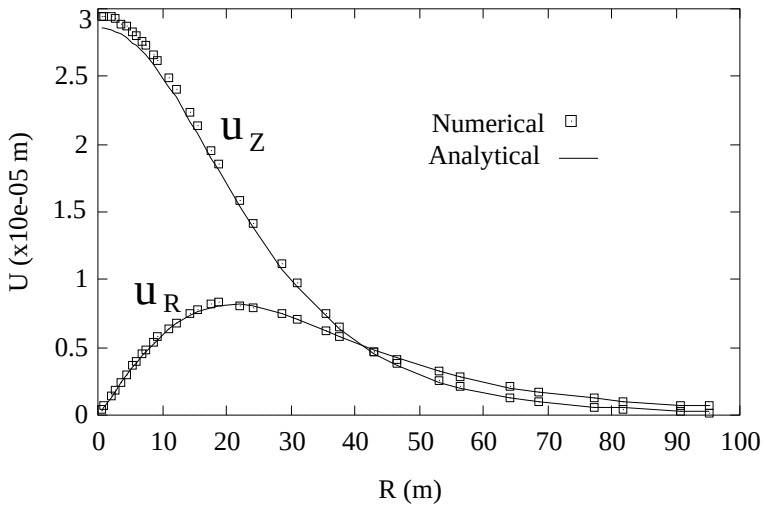

Figure 7: Comparison of displacements for a 638 elements fracture and a circular ground surface

	Square ground surface 800 elements	Square surface 1800 elements	Circular surface 820 elements
Fracture 226 elements	3.5	4.9	6.1
Fracture 638 elements	0.4	1.8	2.7

Table 2: Mean relative errors (%) on ground surface vertical displacements for different discretizations of the fracture and the ground surface. Elements of the ground surface are constant

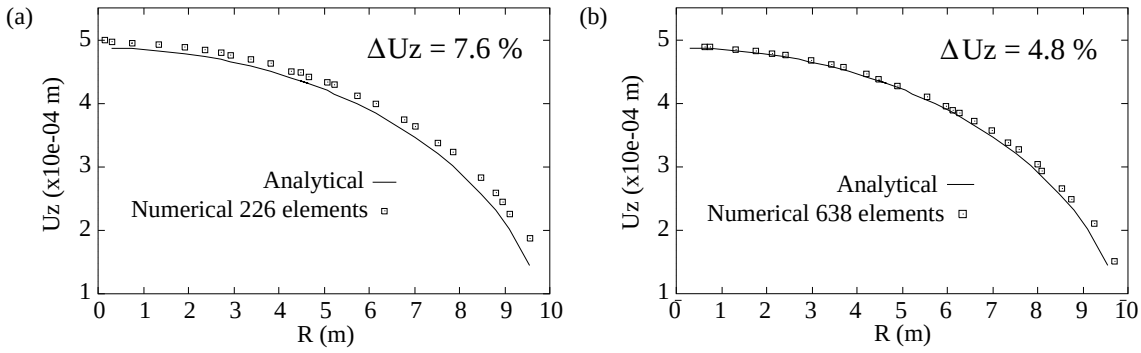

Figure 8: Comparisons of vertical displacements on the fracture. (a) discretization with 226 elements. (b) discretization with 638 elements.

accurately. This hypothesis is verified by comparing vertical displacements found numerically and analytically [28] for a fracture embedded in an infinite medium. For this purpose, the mean relative error on vertical displacement is calculated on the fracture surface,

$$Err\ u_Z(\%) = \frac{1}{N_F} \sum_{\Gamma_F} \left| \frac{u_Z^{analytical} - u_Z^{numerical}}{u_Z^{analytical}} \right| . \tag{38}$$

Figure 8 shows that vertical displacements are overestimated for both discretizations of the fracture, and that overestimation decreases when fracture discretization is increased. Therefore, the overestimation of displacements on the ground surface results from an overestimation of displacements on the fracture. With the circular ground surface, Table 2 shows that, for a given discretization of the fracture, overestimation of vertical displacements is greater than with the square surfaces. In fact, values of overestimations on the circular ground surface are the closest to those on the fracture. This means that the circular graded mesh provides the best match to the displacements on the fracture.

For the next steps of the validation, the 638 element fracture and the circular ground surface will be chosen as they provide the best discretizations.

Validation of the modified row-sum with constant elements

In order to validate the modified row-sum elimination method, results are compared with those found when singular influence coefficients $\mathbf{c}^l + \hat{\mathbf{h}}_{ll}$ are calculated analytically. This comparison is performed for constant elements as analytic evaluation of the $\mathbf{c}^l + \hat{\mathbf{h}}_{ll}$ is fairly simple. Accuracy of the method is evaluated through the mean relative difference between displacements on $\Gamma_F + \Gamma_M$ calculated both ways. For the 638 elements fracture and the circular ground surface, error on u_Z is

$$\Delta\ u_Z = \frac{1}{N_F + N_L} \sum_{\Gamma_F + \Gamma_M} \left| \frac{u_Z^{analytic\ integration} - u_Z^{row-sum}}{u_Z^{analytic\ integration}} \right| = 0.013\% . \tag{39}$$

This proves that the modified row-sum elimination is a very accurate way of estimating singular influence coefficients. Table 3 shows that the row-sum elimination takes only slightly longer time than analytic integration for the calculation of singular influence coefficients.

	Analytic integration	row-sum elimination
Assembly time (sec)	938	1018

Table 3: Comparison of time required for the evaluation of singular coefficients $\mathbf{c}^l + \hat{\mathbf{h}}_{ll}$ on constant elements. Computation is performed on a *Sun* SPARC Station 20

	Row-sum constant elements	Row-sum linear elements
Total solution time (sec)	4804	773
Number of function nodes	1448	1064
Err u_Z (%)	2.7	4

Table 4: Comparisons between solution times and mean relative errors for constant and linear elements

Validation of the modified row-sum with linear elements

As shown in Table 4, total solution time is considerable with constant elements, while the use of linear elements reduces solution time by 84 %. In fact, in this case, the number of function nodes required with linear elements is small enough to avoid disk swapping. Note also that vertical ground displacements found with linear elements overestimate analytical displacements by 4% instead of 2.7% with constant elements. Recalling that displacements on the fracture surface are overestimated by 4.8%, it can be concluded that linear elements better model the fracture. Although paradoxal, this result shows again the importance of a proper discretization of the pressurized boundary.

Intersection of fractures with massive boundaries

In order to investigate the behaviour of the 3D Mixed BEM for the case of a fracture intersecting a massive boundary, comparison is done with results calculated with a 2D BEM by D. D. Pollard et al. [29]. Using this 2D BEM, they calculated vertical surface displacements created by a pressurized crack with a dip of 75 ° that breach the ground surface of an elastic half-space. Using the 3D Mixed BEM, the fracture is modeled with the DD method and constant elements, and the ground surface is modeled with the direct method and linear elements except where it intersects fracture. In this case, constant elements are used for the ground surface. For a valid comparison with two dimensional results, the length L of the fracture is chosen large compared to the height a: $L/a = 12$ (Figure 9) and displacements are calculated on profile A-A' that intersects the fracture in its middle where plane strain can be hypothesized.

Figure 10, shows that plane strain is verified over a distance of approximately $5a$ along the fracture. Figure 11 compares normalized vertical surface displacements versus normalized horizontal distances. Origin of horizontal distances is taken at the intersection between the fracture and the ground surface. Coefficient k used for normalization of

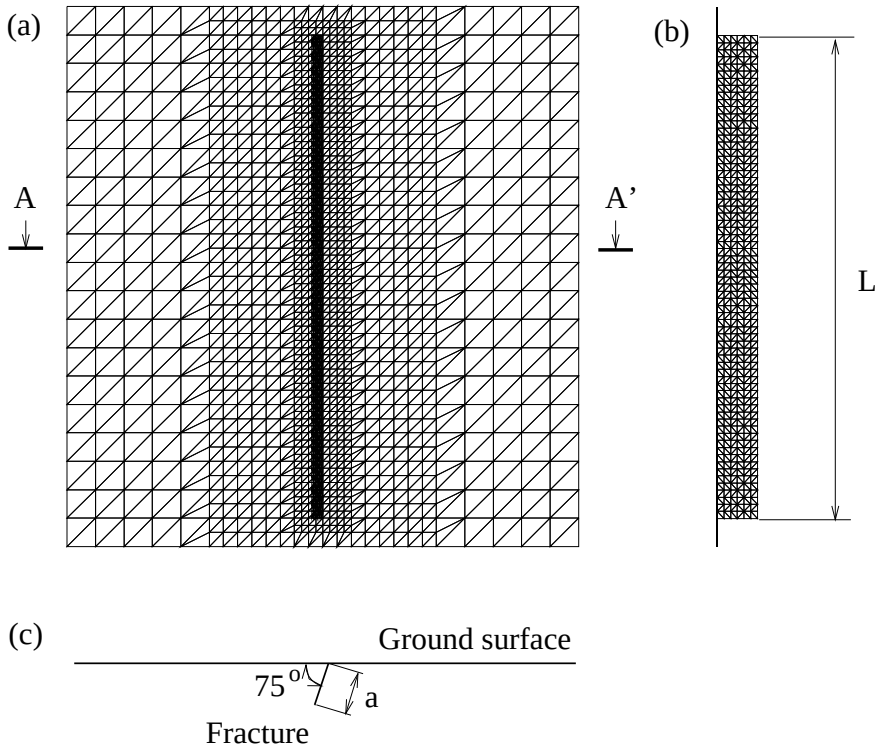

Figure 9: Portion of the mesh used for modeling the intersection of a fracture with a massive boundary. (a) Top view (b) Right cross-section (c) Cross section A-A'

vertical displacements is $\frac{2\ G}{\Delta P\ a\ (1-\nu)\ sin(75°)}$, where ΔP is the driving pressure. Coefficient d used to normalize horizontal distances is the depth of the middle of the fracture below ground surface, $a\ sin(75°)\ /\ 2$.

Vertical displacements calculated with the 3D Mixed BEM are less that those calculated with a 2D BEM. This can be attributed to the coarse discretization: the height a of the fracture is only divided into 6 segments, and discretization of the ground surface is the same as that of the fracture near the fracture, progressively decreasing when going away from it.

CONCLUSIONS

A 3D Boundary Element Method (BEM), which combines the Displacement Discontinuity and the Direct methods has been developed for the analysis of elastic deformation fields of bodies with fractures and surface topographies, as well as pressurized reservoirs. A modified row-sum elimination method has been developed for the calculation of singular influence coefficients when linear elements are used on ground surfaces. It allows fast and reliable computation of solutions.

This Mixed BEM has been tested on the problem of a pressurized circular fracture in an elastic half-space. Good agreement has been found between analytical and numerical results. For this particular problem, the leading importance of a proper discretization of the pressurized boundary (i.e. the fracture), has been outlined. Also, results are more

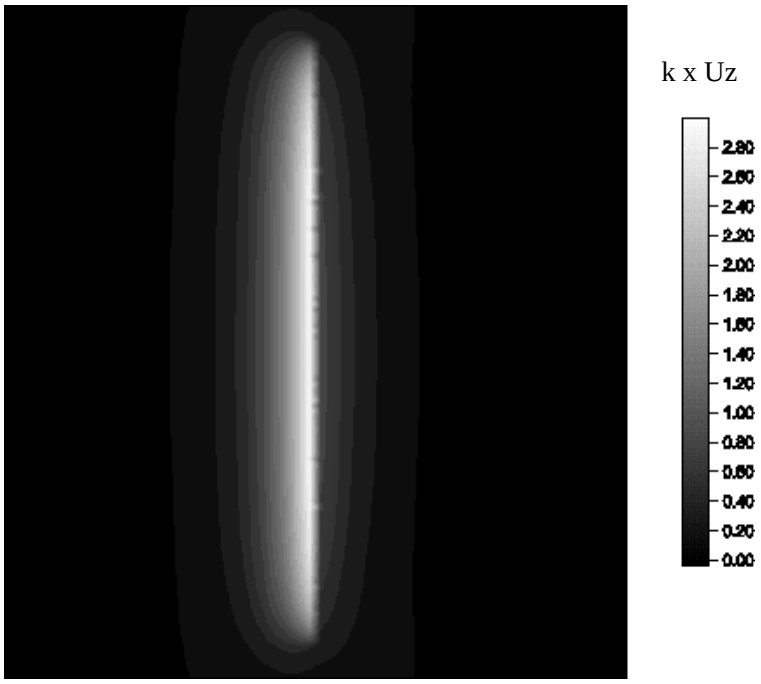

Figure 10: Normalized vertical surface displacements created by an inclined pressurized fracture of dip 75 °.

accurate when the ground surface is represented with a graded mesh, with fine elements in the most perturbed area and coarser elements further, than with a regular mesh. The graded mesh also requires fewer elements. Thus, it is computationally less expensive.

Finally, the Mixed BEM has shown to be valid when two types of elements (DD and Direct method) intersect, provided constant elements are used for parts of massive boundaries adjoining fractures.

APPENDIX

Calculation of singular influence coefficients of DDs in (31) is performed from evaluation of I (17) in the local coordinate system $(x,\ y,\ z)$ such that the z axis is normal to the element plane. Calculation of I [23, 24] on a triangular element with vertices $M_1(x_1,\ y_1,\ 0)$, $M_2(x_2,\ y_2,\ 0)$ and $M_3(x_3,\ y_3,\ 0)$ is performed using the divergence theorem. It gives at $\psi(x,\ y,\ z) \in \Omega$,

$$I = I(\psi) = I(x,y,z) = \sum_{k=1}^{3} I_k + |z|\theta_0 \ , \tag{40}$$

where

$$I_k = \frac{M_k}{L_k}\,(g_k - h_k) + z\left(\arctan(zSb^k) - \arctan(zSa^k)\right),$$

and $0 < \theta_0 < 2\pi$, depending on the location of the projection of ψ on the triangular element. Terms appearing in I_k are

$$M_k = (y_k - y_{k+1})x + (x_{k+1} - x_k)y + x_k y_{k+1} - y_k x_{k+1} \ ,$$

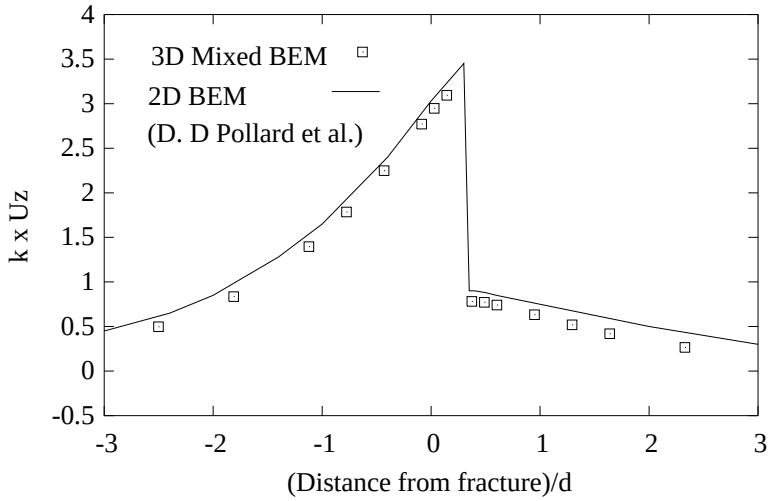

Figure 11: Normalized vertical surface displacements for a pressurized fracture intersecting the ground surface. Dip is 75 °.

$$
\begin{aligned}
L_k &= \sqrt{(x_{k+1}-x_k)^2+(y_{k+1}-y_k)^2}\ , \\
g_k &= \ln\left(B_k + r_{k+1}\right)\ , \\
h_k &= \ln\left(A_k + r_k\right)\ , \\
Sb^k &= \frac{B_k L_k}{M_k r_{k+1}}\ , \\
Sa^k &= \frac{A_k L_k}{M_k r_k}\ ,
\end{aligned}
$$

with,

$$
\begin{aligned}
B_k &= \left[(x_k - x_{k+1})x + (y_k - y_{k+1})y + (x_{k+1}-x_k)x_{k+1} + (y_{k+1}-y_k)y_{k+1}\right]/L_k\ , \\
A_k &= \left[(x_k - x_{k+1})x + (y_k - y_{k+1})y + (x_{k+1}-x_k)x_k + (y_{k+1}-y_k)y_k\right]/L_k\ , \\
r_{k+1} &= \sqrt{(x_{k+1}-x)^2+(y_{k+1}-y)^2+z^2}\ , \\
r_k &= \sqrt{(x_k-x)^2+(y_k-y)^2+z^2}\ .
\end{aligned}
$$

To calculate singular influence coefficients, partial derivatives of I are expressed in the limiting case where the origin of the local coordinate system is at the centroid of the triangular element and $\psi \to (0,0,0)$,

$$
\begin{aligned}
I_{,xx}(0,0,0) &= \sum_{k=1}^{3}\frac{1}{L_k}\left\{2l_k^y\left(g_{,x}^{k}-h_{,x}^{k}\right)+M_k\left(g_{,xx}^{k}-h_{,xx}^{k}\right)\right\}\ , \\
I_{,yy}(0,0,0) &= \sum_{k=1}^{3}\frac{1}{L_k}\left\{-2l_k^x\left(g_{,y}^{k}-h_{,y}^{k}\right)+M_k\left(g_{,yy}^{k}-h_{,yy}^{k}\right)\right\}\ , \\
I_{,zz}(0,0,0) &= \sum_{k=1}^{3}\frac{M_k}{L_k}\left\{g_{,zz}^{k}-h_{,zz}^{k}\right\}+\sum_{k=1}^{3}2\left(Sb^k-Sa^k\right)\ , \\
I_{,xy}(0,0,0) &= \sum_{k=1}^{3}\frac{1}{L_k}\left\{-l_k^x\left(g_{,x}^{k}-h_{,x}^{k}\right)+M_k\left(g_{,xy}^{k}-h_{,xy}^{k}\right)+l_k^y\left(g_{,y}^{k}-h_{,y}^{k}\right)\right\}\ ,
\end{aligned}
$$

$$
\begin{aligned}
I_{,xz}(0,0,0) &= 0 \ , \\
I_{,yz}(0,0,0) &= 0 \ ,
\end{aligned}
$$

with,

$$
\begin{aligned}
l_k^x &= x_k - x_{k+1} \ , \\
l_k^y &= y_k - y_{k+1} \ .
\end{aligned}
$$

Partial derivatives of g^k and h^k with respect to ψ give, for $\psi \to (0,0,0)$,

$$
\begin{aligned}
g^k_{,x} &= \frac{1}{(B_k + r_{k+1})} \left(\frac{l_k^x}{L_k} - \frac{x_{k+1}}{r_{k+1}} \right) \ , \\
h^k_{,x} &= \frac{1}{(A_k + r_k)} \left(\frac{l_k^x}{L_k} - \frac{x_k}{r_k} \right) \ , \\
g^k_{,y} &= \frac{1}{(B_k + r_{k+1})} \left(\frac{l_k^y}{L_k} - \frac{y_{k+1}}{r_{k+1}} \right) \ , \\
h^k_{,y} &= \frac{1}{(A_k + r_k)} \left(\frac{l_k^y}{L_k} - \frac{y_k}{r_k} \right) \ , \\
g^k_{,xx} &= -\frac{1}{(B_k + r_{k+1})^2} \left(\frac{l_k^x}{L_k} - \frac{x_{k+1}}{r_{k+1}} \right)^2 + \frac{1}{(B_k + r_{k+1})} \frac{(y_{k+1})^2}{(r_{k+1})^3} \ , \\
h^k_{,xx} &= -\frac{1}{(A_k + r_k)^2} \left(\frac{l_k^x}{L_k} - \frac{x_k}{r_k} \right)^2 + \frac{1}{(A_k + r_k)} \frac{(y_k)^2}{(r_k)^3} \ , \\
g^k_{,yy} &= -\frac{1}{(B_k + r_{k+1})^2} \left(\frac{l_k^y}{L_k} - \frac{y_{k+1}}{r_{k+1}} \right)^2 + \frac{1}{(B_k + r_{k+1})} \frac{(x_{k+1})^2}{(r_{k+1})^3} \ , \\
h^k_{,yy} &= -\frac{1}{(A_k + r_k)^2} \left(\frac{l_k^x}{L_k} - \frac{y_k}{r_k} \right)^2 + \frac{1}{(A_k + r_k)} \frac{(x_k)^2}{(r_k)^3} \ , \\
g^k_{,zz} &= \frac{1}{(B_k + r_{k+1})} \frac{1}{r_{k+1}} \ , \\
h^k_{,zz} &= \frac{1}{(A_k + r_k)} \frac{1}{r_k} \ , \\
g^k_{,xy} &= -\frac{1}{(B_k + r_{k+1})^2} \left(\frac{l_k^y}{L_k} - \frac{y_{k+1}}{r_{k+1}} \right) \left(\frac{l_k^x}{L_k} - \frac{x_{k+1}}{r_{k+1}} \right) - \frac{1}{(B_k + r_{k+1})} \frac{y_{k+1} x_{k+1}}{(r_{k+1})^3} \ , \\
h^k_{,xy} &= -\frac{1}{(A_k + r_k)^2} \left(\frac{l_k^y}{L_k} - \frac{y_k}{r_k} \right) \left(\frac{l_k^x}{L_k} - \frac{x_k}{r_k} \right) - \frac{1}{(A_k + r_k)} \frac{y_k x_k}{(r_k)^3} \ .
\end{aligned}
$$

aknowledgements- This research was funded in part by CNRS-ECOTEC (ARC Geothermie des Roches Fracturées). Quick implementation of this Mixed method was made possible thanks to J. H. Curran and his team who provided us with the source code of COMPUTE^{3D}, and with the modeling and visualization program EXAMINE^{3D}. Their help is gratefully acknowledged.

References

[1] Salomon M. D. G. Elastic analysis of displacements and stresses induced by the mining of seam or reef deposits, Part I, *J. S. Afr. Inst. Min. Metall.*, **64**, 128-149 (1963).

[2] Ryan M. P. Blevins J. Y. K. Okanamura A. T. and Koyonagi R. Y. Magma reservoir subsidence mechanics: Theoretical summary and application to Kilauea volcano, Hawaii, *J. Geophys. Res.*, **88**, No. 5, 4147-4181 (1983).

[3] King G. C. P. Stein R. S. and Lin J. Static stress changes and the triggering of earthquakes, *Bull. Seism. Soc. Am.*, **84**, No. 3, 935-953 (1994).

[4] Mogi K. Relations between the eruptions of various volcanoes and the deformation of the ground surfaces around them. *Bull. Earthquake Res. Inst., Univ. Tokyo*, **36**, 99-134 (1958).

[5] Dieterich J. H. and Decker R. W. Finite element modeling of surface deformation associated with volcanism. *J. Geophys. Res.*, **80**, 4094-4102 (1975).

[6] Pollard D. D. and Holzhausen G. On the mechanical interaction between a fluid-filled fracture and the earth's surface. *Tectonophysics*, **53**, 27-57 (1979).

[7] Okada Y. Surface deformation due to shear and tensile faults in a half-space. *Bull. Seism. Soc. Am.*, **75**, 1135-1154 (1985).

[8] McTigue D. F. and Segall P. Displacements and tilts from dip-slip faults and magma chambers beneath irregular surface topography. *Geophys. Res. Lett.*, **15**, No. 6, 601-604 (1988).

[9] Rizzo F. J. An integral equation approach to boundary value problems of classical elastostatics. *Quart. Appl. Math*, **25**, 83-95, (1967).

[10] Cruse T. A. Numerical solutions in three-dimensional elastostatics. *Int. J. Solids Struct.*, **5**, 1259-1274 (1969).

[11] Cruse T. A. An improved boundary integral equation method for three-dimensional elastic stress analysis. *Computers & Structures*, **4**, 741-754 (1974).

[12] Lachat J. C. and Watson J. O. Effective numerical treatment of boundary integral equations: a formulation for three- dimensional elastostatics. *Int. J. numer. Meth. Engng.*, **10**, 991-1005 (1976).

[13] Rongved L. and Hill N. J. Dislocation over a bounded plane area in an infinite solid. *J. Appl. Mech.*, **24**, 253-254 (1957).

[14] Crouch S. L. Solution of plane elasticity problems by the displacement discontinuity method. *Int. J. numer. Meth. Engng.*, **10**, 3001-3433 (1976).

[15] Crouch, S. L. and A. M. Starfield. *Boundary Element Methods in Solid Mechanics.* Allen & Unwin, London (1983).

[16] Crawford A. M. and Curran J. H. Higher-order functional variation displacement discontinuity elements. *Int. J. Rock Mech. Min. Sci. & Geomech. Abstr.*, **19**, 143-148 (1982).

[17] Diering T. A. C. Further developments of the Boundary Element Method With Applications in Mining. MSc thesis, University of the Witwatersrand, Johannesburg, South Africa (1981).

[18] Curran J. H. Corkum B. T. and Shah S. *COMPUTE^{3D} BEM, Version 2.23.* Rock Engineering Group, Department of Civil Engineering, University of Toronto (1992-94).

[19] Shah S. Practical implementation of the direct Boundary element method for three-dimensional stress analysis of underground excavations. PhD thesis, University of Toronto (1992).

[20] Curran J. H. and Corkum B. T. *EXAMINE^{3D} Users' Manual, Version 2.0.* Data Visualization Laboratory, Department of Civil Engineering, University of Toronto (1990-93).

[21] Watson J. O. Advanced implementation of boundary element method for two- and three-dimensional elastostatics. In *developments in Boundary Elements Methods.* Applied Science Publishers Ltd., Essex, England, 31-63 (1979).

[22] Kane J. H. Gupta A. and Saigal S. Reusable intrinsic sample point (RISP) for the efficient numerical integration of three- dimensional curved boundary elements. *Int. J. Numer. Meth. Engng.*, **28**, 1661-1676 (1989)

[23] Medina D. E. and Liggett J. A. Three-dimensional boundary-element computation of potential flow in fractured rock. *Int. J. Numer. Meth. Engng.*, **26**, 2319-2330 (1988).

[24] Medina D. E. and Liggett J. A. Exact integrals for three-dimensional boundary element potential problems. *Communications in Applied Numerical Methods*, **5**, 555-561 (1989).

[25] Saad Y. and Schultz M. H. GMRES: a Generalized Minimal Residual algorithm for solving nonsymmetric linear systems. *SIAM J. Sci. Stat. Comput.*, **7**, No. 3, 856-869 (1986).

[26] Sun J. R. Theoretical size of hydraulically induced horizontal fracture and corresponding surface uplift in an idealized medium. *J. Geophys. Res.*, **74**, 5995-6011 (1969).

[27] Touloukian Y. S Judd W. R. and Roy R. F. *Physical Properties of Rocks and Minerals. Data Series on Material Propertie.* Vol 1-2, New York: McGray-Hill (1981).

[28] Sneddon, I. N. The distribution of stress in the neighbourhood of a crack in an elastic solid. *Proc. R. Soc. London, A*, **187**, 229-260 (1946).

[29] Pollard, D. D. Delaney P. T. Duffield W. A. Endo E. T. and Okanamura A. T. Surface Deformation in Volcanic Rift Zones. *Tectonophysics*, **94**, 541-584, 1983.